Reaction of Pentadienyl Complexes with Metal Carbonyls: Synthetic, Structural, and Theoretical Studies of Metallabenzene π-Complexes

Ulrike Effertz,[†] Ulli Englert,[†] Frank Podewils,[†] Albrecht Salzer,*[,†] Trixie Wagner,[†] and Martin Kaupp*[,‡]

Institut für Anorganische Chemie der RWTH Aachen, D 52056 Aachen, Germany, and Institut für Anorganische Chemie, Universität Würzburg, Am Hubland, D 97074 Würzburg, Germany

Received September 20, 2002

The reaction of open and half-open sandwich complexes of iron and ruthenium with metal carbonyls was studied. Three types of complexes could be isolated: Carbonyl-bridged iron−ruthenium dimers with cyclopentadienyl and pentadienyl terminal ligands, dimetallic iron carbonyl complexes with a bridging σ,π-coordinated pentadienyl ligand, and ruthenium complexes with one or two π-coordinated ruthenabenzene ligands. The latter are the first ever isolated bis(metallabenzene) π-complexes. The X-ray structures of $C_5Me_5Ru(CO)_4Fe(C_7H_{11})$, $(\mu\text{-}C_7H_{10})Fe_2(CO)_6$, and $[(C_8H_{11})Ru(CO)_3]_2Ru$ are reported. Density functional calculations have been used to better understand the bonding in metallabenzene complexes. The electron localization function (ELF) clearly confirms metal−metal bonding interactions in the complexes studied. In particular, the bis(metallabenzene) complex **13** is found to exhibit a three-center bonding attractor in the ELF in its stable syn-eclipsed conformation but two two-center attractors in the ca. 30 kJ mol^{-1} less stable anti-eclipsed arrangement. The frontier orbitals of metallabenzenes exhibit very large participation of the ring metal. When metallabenzenes act as ligands to other metal fragments, direct metal−metal interactions are thus expected to be a general feature of the complexes, unless they are replaced by other interactions, e.g. by protonation. Natural population analyses suggest that the σ-donor abilities of the electron-rich d^8 metallabenzene fragments predominate over their π-acceptor character.

Introduction

In earlier papers, we have discussed the reaction of "half-open" metallocenes with organometallic fragments, which by insertion into the "open" side of pentadienyl ligands in some cases led to rare examples of metallabenzenes π-coordinated to a second transition metal.[1−3] This reaction can be regarded as the expansion of an arachno to a nido structure, using the terminology developed by Wade.[4] Metallabenzenes thus formed (isolobal exchange of CH for a metal fragment) are still relatively rare species. Their chemistry has recently been extensively reviewed by Bleeke.[5] They are postulated as intermediates in the alkyne polymerization[6] but are also of fundamental interest with respect to their possible aromatic character.[5−7] Related heterocycles of the main groups, formed by isolobal exchange of CH for BH^- or P, are on the other hand well-known and their coordination chemistry has been studied in great detail in the last 30 years. They are very suitable as ligands for metal-sandwich complexes, in particular for triple-decker and multidecker compounds.

The synthesis of metallabenzenes by the insertion route remains unfortunately a poorly understood and unpredictable reaction. We have undertaken a broad study of the reaction of "half-open" and "open" metallocenes of iron and ruthenium with metal carbonyls to find more examples of metallabenzene complexes.

We will use density functional theory (DFT) and various types of electronic-structure analyses to study bonding in a number of metallabenzene complexes. The bonding in metallabenzenes has aroused interest since the first examples of such systems were reported. The main issue has been the question of the aromaticity of the cyclically delocalized electronic system. Structural and NMR data suggest that the bonding in metallabenzene rings does indeed exhibit aromatic character. This is supported by bonding studies, which however suggest less aromatic character than in benzene, due to the polar character of the metal−carbon bonds.[4,7] Indeed, Thorn and Hoffmann[7] predicted heteroaromaticity and thus enhanced stability for a number of metallabenzenes in a seminal paper in 1979, when almost no examples of stable metallabenzenes were known experimentally. In this study we will touch upon the aromaticity issue only briefly. Our main emphasis will

[†] Institut für Anorganische Chemie der RWTH Aachen.
[‡] Universität Würzburg.

(1) Bosch, H. W.; Hund, U.; Nietlispach, D.; Salzer, A. *Organometallics* **1992**, *11*, 2087.
(2) Bertling, U.; Englert, U.; Salzer., A. *Angew. Chem.* **1994**, *106*, 1026; *Angew. Chem., Int. Ed. Engl.* **1994**, *33*, 1003.
(3) Englert, U.; Podewils, F.; Schiffers, I.; Salzer. A. *Angew. Chem.* **1998**, *110*, 2196; *Angew. Chem., Int. Ed.* **1998**, *37*, 2134.
(4) Wade, K. *Adv. Inorg. Chem. Radiochem.* **1976**, *18*, 1.
(5) Bleeke, J. R. *Chem. Rev.* **2001**, *101*, 1205.
(6) Lin, W.; Wilson, S. R.; Girolami, G. *OrganometalIics* **1997**, *16*, 2356.
(7) Thorn, D. L.; Hoffmann, R. *Nouv. J. Chim.* **1979**, *3*, 39.

10.1021/om020789h CCC: $25.00
Publication on Web 12/13/2002

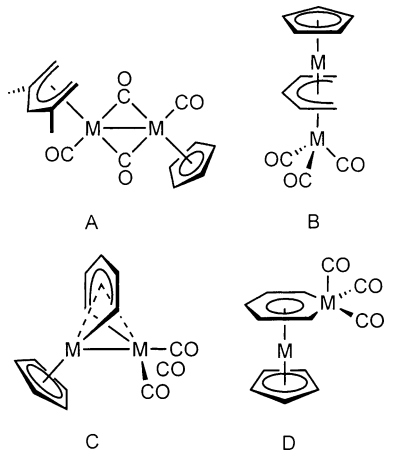

Figure 1. Possible dimers from the reaction of half-open metallocenes with metal carbonyls.

be on the bonding in metallabenzene complexes: in particular, on the question of whether direct metal−metal interactions occur and whether in such complexes metallabenzenes are better characterized as σ-donor or π-acceptor ligands. We will also address the nonplanarity of the metallabenzene rings in the complexes, the syn-eclipsed arrangement of the two rings in **13**, and the preferred protonation site of **13**.

Synthetic Results

In our previous studies, we had used the triple-decker complex $[Ni_2Cp_3]^+$ and $[CpRu(CH_3CN)_3]^+$ as precursors for the 14e fragment $[CpNi]^+$ and 12e fragment $[CpRu]^+$, respectively.[1,2] Further attempts to use other unsaturated fragments such as $[C_5Me_5Ru]^+$, $[C_5Me_5Fe]^+$, $[CODRh]^+$, [CpCo], $[C_5Me_5Co]$, and [CpRh], formed from various precursors, were unsuccessful. Either there was no reaction or a mixture of compounds was formed that was neither separable nor identifiable.

Metal carbonyls as starting materials have a possible advantage over other precursors in that they can react in a stepwise fashion, releasing several CO ligands consecutively. They are also capable of CH-activation reactions, a necessary requirement for the insertion into the open face of pentadienyl complexes. Considering the general reactivity of pentadienyl compounds, we anticipated the possible formation of several different structural types of dimetallic compounds on reaction of half-open metallocenes with metal carbonyls (Figure 1).

We have therefore treated a variety of pentadienyl sandwich complexes, $C_5Me_5Fe(dmp)$ (**1**; dmp = 2,4-dimethylpentadienyl), $C_5Me_5Fe(tmp)$ (**2**; tmp = 2,3,4-trimethylpentadienyl), $C_5Me_5Ru(dmp)$ (**3**), $C_5Me_5Ru(tmp)$ (**4**), $Fe(dmp)_2$ (**5**), $Fe(tmp)_2$ (**6**), $Ru(dmp)_2$ (**7**), and $Ru(tmp)_2$ (**8**), with the homoleptic carbonyls of Cr, Mo, Re, Mn, Fe, and Ru in general under reflux conditions. In many cases no identifiable products or previously known compounds were obtained. Thus, the treatment of **2** with $Mn_2(CO)_{10}$ gave $C_5Me_5Mn(CO)_3$[8] and $(dmp)Mn(CO)_3$[9] as the only isolable products. Reaction of **1** with $Ru_3(CO)_{12}$ gave $[C_5Me_5Fe(CO)_2]_2$.[10]

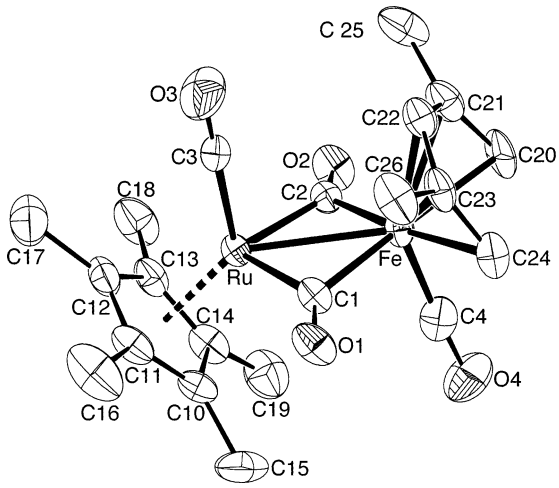

Figure 2. PLATON view of complex **9** with 50% displacement ellipsoid probability. H atoms are omitted.

Scheme 1

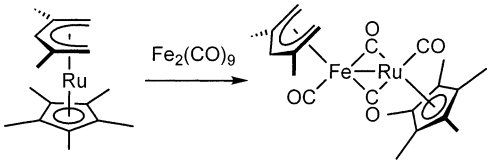

Novel complexes were obtained on reacting **3** and **4** with $Fe_2(CO)_9$. We were able to isolate the heterobimetallic complexes $C_5Me_5Ru(CO)_4Fe(dmp)$ (**9**) and $C_5Me_5Ru(CO)_4Fe(tmp)$ (**10**) in 80% and 39% yields, respectively, as orange-red air-stable crystals (Scheme 1).

The IR spectra showed resonances for both terminal and bridging carbonyls. Suitable crystals of **9** could be obtained by crystallization from diethyl ether. The X-ray structure (Figure 2) shows a dimer with two bridging and two terminal carbonyl groups in a trans arrangement, the C_5Me_5 ring being coordinated to ruthenium and the dmp ligand to iron. The structure is very similar to that of the well-known dimeric C_5H_5 and C_5Me_5 iron and ruthenium carbonyls.

The formation of these complexes clearly involves a relatively complicated route, and it is likely that intermediates are formed in which the dmp and tmp ligands act as bridging ligands before being fully transferred to iron. The "open" pentadienyl ligand is more susceptible to migration reactions, due to its structural flexibility and its ability to also bind via the η^1 and η^3 bonding modes. Reaction routes involving monometallic fragments $C_5Me_5Ru(CO)_2$ and $(dmp)Fe(CO)_2$ seem unlikely, as we have found no evidence for symmetrical coupling products.

The dimeric species $[(dmp)Fe(CO)_2]_2$ is known, and its X-ray structure has been described by Ernst.[11] In contrast to **9**, this compound shows a cis arrangement of the dienyl and carbonyl terminal ligands. The compound $[(dmp)Ru(CO)_2]_2$ is as yet unknown. We have not been able to prepare it by refluxing $Ru_3(CO)_{12}$ with dmp.

On treating **5** and **6** with $Fe_2(CO)_9$, we were also able to isolate two dimetallic species **11** and **12** in reasonable yields as orange-red crystals. These compounds again

(8) King, R. B.; Efraty, A. *J. Am. Chem. Soc.* **1972**, *94*, 3773.
(9) Kreiter, C. G.; Leyendecker, M. *J. Organomet. Chem.* **1985**, *280*, 225.
(10) Zou, C.; Wrighton, M. S.; Blaka, J. P. *Organometallics* **1987**, *6*, 1452.
(11) Gedridge, R. W.; Patton, A. T.; Ernst, R.; Ma, H. *J. Organomet. Chem.* **1987**, *331*, 73.

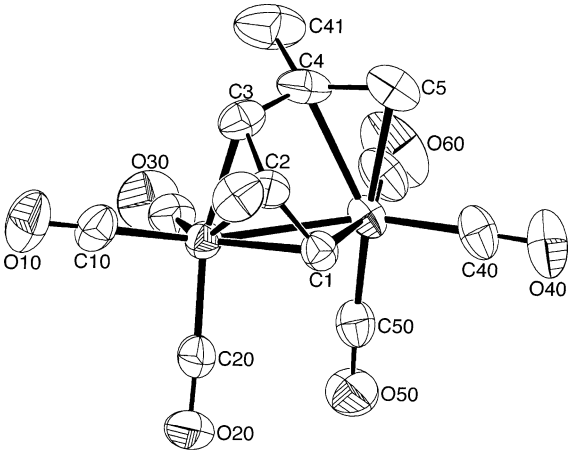

Figure 3. PLATON view of complex **11** with 50% displacement ellipsoid probability. H atoms are omitted.

Scheme 2

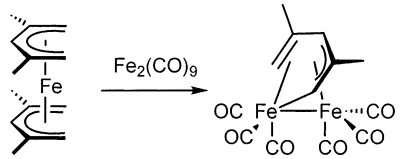

5 **11**

were very stable and could even be purified via sublimation (Scheme 2).

The IR spectra showed no signals due to bridging carbonyls. The ^{1}H NMR for **11** had resonances for an unsymmetrically coordinated dimethylpentadienyl ligand in a ratio of 1:1:3:3:1:1, with an unusual low-field shift at 6.68 ppm. This proton was correlated to a carbon atom showing a resonance at 147 ppm. These shifts were reminiscent of the low-field shifts in "fly-over" complexes.[12] Single crystals of **11** were grown via high-vacuum sublimation using a small temperature gradient (50−25 °C). The X-ray structure is shown in Figure 3.

Compound **11** is a dimetallic complex with an unsymmetrical "fly-over" coordination of the pentadienyl ligand, which has lost one hydrogen atom. One iron atom is σ,π-coordinated to the bridging ligand, while the other iron is bonded in a π-allyl fashion. One terminal carbon atom, which has lost one hydrogen atom, is bridging both metal atoms and gives rise to the unusual low-field chemical shift. The structure of **12** is similar to that of **11**.

These compounds can be regarded as insertion products arrested halfway in the formation of a metallabenzene. Why is no second insertion, completing the ferrabenzene ring, observed? Electron counting reveals that the metallabenzene $C_7H_9Fe(CO)_3$, π-coordinated to a second $Fe(CO)_3$ group, would have an uneven number of valence electrons. To get the correct electron count, the ring should have one carbon less, giving a ferrole, and indeed a dimetallic complex with such structure has long been known. It is formed by the reaction of acetylene with iron carbonyl and has the formula (μ-C_4H_4)$Fe_2(CO)_6$.[13]

Treatment of **5** and **6** with $Ru_3(CO)_{12}$ gave no isolable products, and the same was true for reaction of **7** and **8** with $Fe_2(CO)_9$. Reaction of **7** with $Ru_3(CO)_{12}$ in refluxing octane took a completely different course and allowed the isolation of lemon yellow **13** in 18% yield. We have reported the synthesis and structure of **13** in a short communication.[3]

We have performed a similar reaction with **8** and $Ru_3(CO)_{12}$ in refluxing nonane and were able to isolate **14** in 5% yield only (Scheme 3).

13 and **14** are air-stable and decompose only above 150 °C; they can be sublimed under high vacuum at 90 °C. The simple ^{13}C spectra suggested highly symmetrical structures with two nonequivalent carbonyl groups in a ratio of 1:2. Three signals were in a typical region for π-coordinated aromatic ligands, although with pronounced low-field shifts. The mass spectra showed characteristic peaks due to the consecutive loss of six CO ligands and also the formation of tetramethylruthenocene and hexamethylruthenocene, respectively.

Single crystals of **13** and **14** were grown from benzene solutions. Both structures are very similar and confirm the unprecedented formation of bis(metallabenzene) sandwich complexes (Figures 4 and 5).

The two rings in **13** show an exact syn-eclipsed conformation. Both rings are, however, not coplanar. The planes are tilted toward each other with an angle of 18.2°, while the two $Ru(CO)_3$ units are bent away by 14.3 and 16.3° from the plane defined by four coplanar ring carbons, while the carbon atom opposite to the metal atom is bent the other way toward the central ruthenium atom. The methyl groups, although in a sterically unfavorable eclipsed conformation, are nevertheless bent by 7° toward each other. Various explanations have been sought for the nonplanarity of coordinated metallabenzenes, such as optimization of Ru−Ru bond lengths[1,2] or steric repulsion between the substituents at the ring metals.[6] The latter explanation cannot account for the geometry of **13** and **14**, as clearly

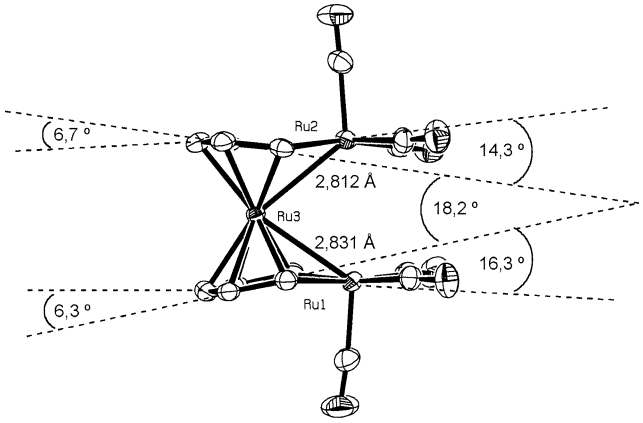

Figure 4. Some relevant interplanar angles in the structure of **13** (methyl groups omitted for clarity).

Scheme 3

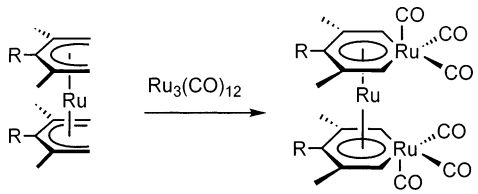

7 R = H
8 R = Me

13 R = H
14 R = Me

(12) Geiger, W. E.; Salzer, A.; Edwin. J.; von Philipsborn, W.; Piantini, U.; Rheingold, A. L. *J. Am. Chem. Soc.* **1990**, *112*, 7113.
(13) Hübel, W.; Weiss, E. *Chem. Ind.* **1959**, 703.

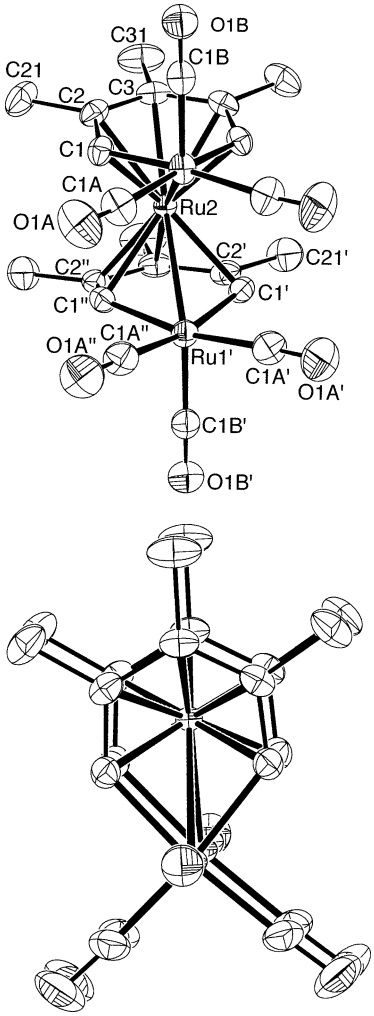

Figure 5. Two PLATON views of complex **14** with 50% displacement ellipsoid probability. H atoms are omitted.

there is no steric repulsion between the carbonyl groups. The Ru−Ru distance between the rings is 3.38 Å in **13**, which is therefore smaller than the sum of the van der Waals radii, while the Ru−Ru bond lengths to the central ruthenium atom are 2.82 Å. While many sandwich complexes with heterobenzene ring ligands show either a preferred anti orientation or low barriers of rotation with disordered structures,[14,15] comparable syneclipsed structures have been found for distiba- and dibismaferrocenes.[16] Here again the Sb−Sb and Bi−Bi distances are smaller than the sum of the van der Waals radii and bonding interactions between these heteroatoms have been inferred.

The three carbonyl groups and the two Ru−C ring bonds form a distorted square pyramid. The axial position is occupied by a carbonyl group, whose Ru−C bond length is 1.87 Å. The two other CO groups in equatorial positions have considerably longer Ru−C bonds (1.96 Å), consistent with a trans effect of the pentadienylylidene ligand. The five IR resonances of the carbonyl groups in solution are consistent with retention of symmetry class C_{2v} observed in the solid state. We have not found any evidence for ring rotation in solution by variable-temperature NMR, but we cannot exclude that it occurs. There is no exchange of the carbonyl groups on the NMR time scale.

Scheme 4

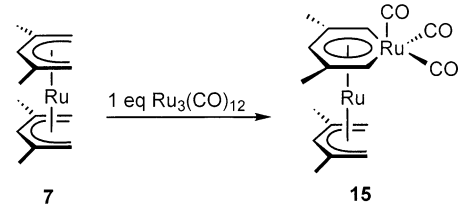

7 **15**

Scheme 5

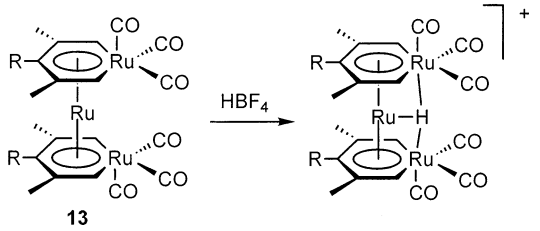

13

As generally observed for metallabenzenes, the C−C bond lengths within the metallcycle are very similar (1.39−1.43 Å), while the Ru−C bond lengths are somewhat longer than in previous examples.[1,2,6]

The solid-state structure of **14** is strikingly similar to that of **13**, although a syn-eclipsed conformation would appear to be even less favorable (Figure 5). The molecule shows crystallographic C_{2v} symmetry.

We have tried to optimize the synthesis by using different ratios of **7** and $Ru_3(CO)_{12}$. On using equimolar amounts, we were able to isolate the monoinsertion product **15**, albeit only in 1% yield. The spectra of **15** are very similar to **13**. This result suggests that the insertion runs in two consecutive steps, **15** being an intermediate on the route to **13** (Scheme 4).

As **13** and **14** are structurally similar to classical metallocenes, we also probed their reactivity. In contrast to ruthenocene, **13** is very easily protonated, a solid cation being isolable. This shows a signal at δ −16.1 ppm in the ^{1}H NMR, typical for a metal hydride (Scheme 5). **13** can also be reversibly oxidized by cyclic voltammetry, (+0.8 V against SCE). While ruthenocene does not undergo a reversible one-electron oxidation, decamethylruthenocene does at a slightly lower value (0.55 V).[17]

As **13** and **14** can be regarded as analogous to boratabenzene complexes, as mentioned before, in that the ligand $[C_5H_5Ru(CO)_3]^-$ is isoelectronic with $[C_5H_5BR]^-$, we have attempted to transfer the ruthenabenzene anion by cleaving it from the complex. Treatment with potassium cyanide in refluxing acetonitrile and reaction with metal precursors such as $[CODRh]^+$ and $[C_5Me_5Rh]^{2+}$ failed to give isolable products, so that it does not seem likely that the ruthenabenzene anion has a stability similar to that of the boratabenzene anion. Attempts to metalate complex **13** also failed, and only decomposition was observed. Treatment of **13** with alkylphosphines in the NMR tube showed moderate reactivity on heating, but with indiscriminate and incomplete substitution of some carbonyl ligands.

(14) Herberich, G.; Ohst, H. *Adv. Organomet. Chem.* **1986**, *25*, 199.
(15) Elschenbroich, C.; Kroker, J.; Massa, W.; Wünsch, M.; Ashe, A. J., III. *Angew. Chem.* **1986**, *98*, 562; *Angew. Chem., Int. Ed. Engl.* **1986**, *25*, 571.
(16) Ashe, A. J., III; Al-Ahmad, S. *Adv. Organomet. Chem.* **1996**, *39*, 325.
(17) Kölle, U.; Salzer, A. *J. Organomet. Chem.* **1983**, *243*, C27.

Table 1. Crystal Data, Data Collection Parameters, and Convergence Results for 9, 11 and 14

	9	11	14
formula	$C_{21}H_{26}FeO_4Ru$	$C_{13}H_{10}Fe_2O_6$	$C_{28}H_{28}O_6Ru_3$
fw	499.36	374.92	763.74
cryst syst	triclinic	orthorhombic	orthorhombic
space group (No.)	$P\bar{1}$ (2)	*Pbca* (61)	*Cmcm* (63)
a, Å	9.484(8)	13.130(7)	11.422(5)
b, Å	14.391(8)	14.011(2)	18.228(14)
c, Å	8.008(5)	15.779(3)	13.299(5)
α, deg	97.87(7)		
β, deg	105.41(6)		
γ, deg	78.86(6)		
U, Å^3	1029.6(12)	2902.8(17)	2769(3)
Z	2	8	4
d_{calcd}, gcm^{-3}	1.61	1.26	1.83
μ, cm^{-1}	14.45	20.20	16.55
θ_{max}, deg	28.0	27.0	28.0
temp, K	258	263	203
λ, Å	0.71073	0.71073	0.71073
cryst dimens, mm^3	0.6 × 0.2 × 0.1	0.3 × 0.25 × 0.2	0.3 × 0.3 × 0.1
abs cor	empirical ψ	empirical ψ	empirical ψ
no. of rflns	4194	3541	5401
no. of indep rflns	3848	3143	1817
no. of variables	251	208	108
R1[a]	0.0622	0.0413	0.0225
wR2[b]	0.1733	0.1420	0.0556
GOF[c]	1.093	1.094	1.080
res electron dens, e Å^{-3}	1.59 (close to Ru)	1.13	0.63

[a] $R1 = \sum||F_o| - |F_c||/\sum|F_o|$, based on data with $I > 2\sigma(I)$. [b] $wR2 = [\sum w(F_o^2 - F_c^2)^2/\sum wF_o^2]^{1/2}$, based on all data. [c] $GOF = [\sum w(F_o^2 - F_c^2)^2/(n_{observns} - n_{var})]^{1/2}$; $n_{observns}$ = no. of observations, n_{var} = no. of variables refined.

In summary, our preparative study on the reaction of metal carbonyls with pentadienyl compounds has in some cases produced very unusual compounds, demonstrating the susceptibility of the pentadienyl ligand to undergo migration and insertion reactions.

Quantum-Chemical Results

Structure Optimizations. Table 2 compares the computed structure parameters for the free metallabenzene $[pdRu(CO)_3]^-$ (pd = pentadienylylidene, C_5H_5) and for the complexes $[\eta^6\text{-}pdRu(CO)_3]_2Ru$ (**13a**) and **13** to the results of the X-ray structure analysis of **13**. The agreement between computed and experimental structural data for **13** may be regarded as excellent, within the range of accuracy expected at the given computational level. While the optimizations for the free metallabenzene suggest an almost planar metallabenzene ring, the calculations of the model complexes generally confirm the experimentally observed bending of the metal fragments away from each other, as well as the tilting of the two ring planes toward each other (Table 2). Although no symmetry restrictions were employed, the optimizations converged to the experimentally determined syn-eclipsed arrangement of the two metallabenzenes in the bis(metallabenzene) sandwich complexes, with C_{2v} symmetry. This suggests an energetic preference for this orientation and electronic interactions favoring the observed eclipsed structure (cf. discussion below). Differences between the computed structures for **13** and **13a** are restricted mainly to the Ru_c−C2(pd) distances; i.e., methyl substitution does slightly lengthen this contact (the Ru_t−Ru_t distance contracts slightly upon substitution). In the unsubstituted model **13a**, the nonplanarity of the metallabenzene ring is only very slightly less pronounced than in **13**. We have also optimized the structure of **13a** in the unknown anti-eclipsed conformation (Table 2; values in parentheses). The optimization in C_s symmetry gave a minimum on the potential energy surface, which however was ca. 29 kJ mol^{-1} less stable than the experimentally observed syn-eclipsed conformation. In the anti-eclipsed conformation, the three ruthenium atoms are almost aligned on a straight line. Hence, the distance between the two Ru_t atoms is maximized, and no direct bonding interaction between them is expected (see below). Experimentally, we have found no evidence for a rotation of the metallabenzene rings in **13** against each other within the temperature range studied. This might suggest that the syn and anti minima on the potential energy surface are connected by a transition state at significantly higher energy. The search for this transition state is outside the scope of the present study.

In comparison to the free metallabenzene anion, the complexes exhibit a somewhat expanded coordination sphere around the metal and longer C−C bonds within the metallabenzene. The most notable difference pertains to the square-pyramidal metal coordination: in comparison to the free metallabenzene, the metal is displaced significantly less from the basal plane made up of C1, C1′, and the two equatorial carbonyl carbon atoms (Table 2). The nonplanarity of the metallabenzene ring in the complex appears to be intimately connected to a change in the coordination of the ring metal. While most of the other dimensions do not differ very much between syn and anti arrangements of the terminal Ru atoms, we note that the buckling of the ring in the anti conformer is less pronounced, whereas the displacement of the metal from the plane is more pronounced than in the more stable syn-ecplised conformer.

Table 3 compares the computed structural data for the cationic nickelabenzene complex $[\{\eta^6\text{-}pdNi(Cp)\}\text{-}RuCp]^+$ (pd = pentadienylylidene) and the experimental data for the substituted analogue $[\{(\eta^6\text{-}dpd)Ni(Cp)\}\text{-}RuCp^*]^+$ (dpd = dimethylpentadienylylidene, C_7H_9).[2] Again, the agreement between theory and experiment may be considered excellent. The Ni−C(Cp) distances in the calculations span a somewhat larger range than found experimentally. The larger distances pertain to the side on which the nickelabenzene coordinates to the ruthenium. The range of the Ru−C(Cp*) distances is generally more restricted, both computationally and experimentally. Table 3 also provides the optimized structural data of the neutral fragment [pdNi(Cp)], which may be considered as the appropriate d^8 metallabenzene analogue to the abovementioned anionic $[pdRu(CO)_3]^-$. Coordination to form a metallabenzene complex again expands the metal coordination shell and also lengthens the C−C bonds within the metallacycle. The range of Ni−C(Cp) distances in the fragment is much narrower than in the complex. This suggests that the coordination of the metallabenzene forces the Cp ring to deviate from ideal η^5 coordination.

Bonding Analyses. Plots of the electron localization function (ELF)[21] provide evidence for metal−metal

(18) Wilson, D. R.; Ernst, R. D.; Cymbaluk, T. H. *Organometallics* **1983**, *2*, 1220.

Table 2. Comparison of Computed and Experimental Structure Parameters for Ruthenabenzene Complexes[a]

param	//B3PW91 [pdRu(CO)$_3$]$^-$	//B3PW91 [pdRu(CO)$_3$]$_2$Ru[b]	//B3PW91 [dpdRu(CO)$_3$]$_2$Ru	[dpdRu(CO)$_3$]$_2$Ru exptl
Ru_c-Ru_t		2.862 (2.840)	2.860	2.811,2.831
Ru_t-Ru_t		3.540 (5.680)	3.499	3.382
Ru_t−C1(pd)	2.041	2.062 (2.042)	2.064	2.061−2.074
$Ru_t-C(CO_{ax})$	1.852	1.857 (1.864)	1.856	1.863, 1.871
$Ru_t-C(CO_{eq})$	1.927	1.949 (1.949)	1.947	1.939−1.965
Ru_c−C1(pd)		2.207 (2.253)	2.192	2.174−2.181
Ru_c−C2(pd)		2.229 (2.205)	2.259	2.244−2.262
Ru_c−C3(pd)		2.205 (2.210)	2.207	2.202
C1−C2	1.392	1.406 (1.407)	1.409	1.393−1.409
C2−C3	1.399	1.423 (1.422)	1.427	1.400−1.433
C2−C(CH_3)			1.509	1.507−1.517
C−O (ax)	1.157	1.145 (1.145)	1.145	1.122, 1.130
C−O (eq)	1.154	1.141 (1.142)	1.142	1.122−1.147
$\angle Ru_t-Ru_c-Ru_t$		76.4 (180.0)	75.4	73.6
C1−C2−C2′-C3[c]	0.5	3.7 (0.2)	5.5	6.3
C2−C1−C1′-Ru[c]	4.5	14.4 (9.1)	15.9	14−16
displ (Ru_t)[d]	0.34	0.18 (0.28)	0.17	0.13

[a] Distances in Å and angles in deg. Averages of numerically (very) slightly different values are provided for the computed results; ranges are given for the experimental data. Abbreviations: Ru_t = terminal Ru atom, Ru_c = central Ru atom, pd = pentadienylylidene, dpd = dimethylpentadienylylidene. [b] Values for the anti conformation in parentheses (cf. also Figure 6b). [c] Difference to 180° dihedral angle provided. [d] Displacement (in Å) of the Ru_t metal from the average plane made up from C1, C1′, and the two equatorial carbonyl carbon atoms.

Table 3. Comparison of Computed and Experimental Structure Parameters for Nickelabenzene Complexes[a]

param	//B3PW91 [pdNi(Cp)]	//B3PW91 {[pdNi(Cp)]-RuCp}$^+$	{[dpdNi(Cp)]RuCp*}$^+$ exptl
Ni−Ru		2.563	2.554
Ni−C1(pd)	1.816	1.850	1.838, 1.867
Ni−C(Cp)	2.13−2.15	2.05−2.21	2.03−2.14
Ru−C1(pd)		2.137, 2.141	2.103, 2.111
Ru−C2(pd)		2.227, 2.223	2.234, 2.222
Ru−C3(pd)		2.234	2.242
Ru−C(Cp)		2.19−2.23	2.18−2.22
C1−C2	1.379	1.405	1.377, 1.408
C2−C3	1.402	1.420	1.425, 1.455
C1−C2−C2′-C3	0.0	2.6	2.5
C2−C1−C1′-Ni	0.1	6.0	7.0

[a] Distances in Å and angles in deg. Averages of numerically (very) slightly different values are provided for the computed results; ranges are given for the experimental data and for M−C(Cp) distances.

interactions in the metallabenzene complexes. In the case of [η^6-dpdRu(CO)$_3$]$_2$Ru (**13**) and its analogue model **13a**, without methyl substituents on the pentadiene, a trisynaptic attractor (a maximum) has been located on the bisector of the $Ru_t-Ru_c-Ru_t$ angle, with a maximum ELF value of ca. 0.42. This attractor, which exhibits distances of ca. 1.79 (1.80) Å from Ru_c and ca. 1.81 (1.83) Å from Ru_t in **13** (**13a**), respectively, is visualized in the isosurface plot for **13a** in Figure 6a. It clearly indicates a three-center bonding situation between the three metal atoms. While the maximum ELF value of the attractor may seem very low, it is just in the range observed previously for transition-metal multicenter bonding[22,23] (see also MO analyses below). In contrast, Figure 6b shows that the attractor is split into two disynaptic attractors in the anti conformer (maximum ELF value 0.38). The two attractors are somewhat off the Ru_t-Ru_c vector, with an attractor−Ru_t-Ru_c angle of 24.6° (and an attractor−Ru_c-Ru_t angle of 22.3°; attractor−Ru_t and attractor−Ru_c distances are 1.621 and 1.473 Å, respectively). Although it is difficult to infer directly from the ELF, it appears reasonable to assume that the additional interaction between the two Ru_t atoms in a three-center situation is responsible for the preference for a syn-eclipsed arrangement in **13**, **13a**, and **14**.

Similarly, Figure 7 demonstrates a Ni−Ru bonding attractor in the ELF for [{[η^6-pdNi(Cp)}RuCp]$^+$, with a maximum value of 0.38. It is located 1.29 Å from Ni and 1.45 Å from Ru and is displaced significantly from the straight line Ni−Ru (the attractor−Ni−Ru angle is 22.4°, and the attractor−Ru−Ni angle is 19.8°). The ELF suggests, thus, that in all metallabenzene complexes studied here direct metal−metal bonding is involved to some extent. Further below, the origin of these interactions is rationalized in terms of frontier orbitals.

Figure 8 shows a top view of an ELF = 0.65 isosurface for the Ni complex in comparison to an analogous plot for benzene. At this higher ELF value, the "heterobenzene" character of the metallabenzene is clearly visible. Very similar pictures are found for the other complexes and for the free metallabenzene fragment anions. While the envelope of the C−C bonding attractors clearly demonstrates the essentially nonpolar character of the bonds, the metal−carbon bonds are strongly polarized toward the carbon atoms. The contours in the carbon part of the metallacycle are expanded in comparison to

(19) Stahl, L.; Ma, H.; Ernst, R. D.; Hyla-Krispin, F.; Gleiter, R.; Ziegler, M. L. *J. Organomet. Chem.* **1987**, *326*, 257.
(20) Bauer, A.; Englert, U.; Geyser, S.; Podewils, F.; Salzer, A. *Organometallics* **2000**, *19*, 5471.
(21) See, e.g.: Becke, A. D.; Edgecombe, K. E. *J. Chem. Phys.* **1990**, *92*, 5397. Savin, A.; Becke, A. D.; Flad, J.; Nesper, R.; von Schnering, H. G. *Angew. Chem.* **1991**, *103*, 421; *Angew. Chem., Int. Ed. Engl.* **1991**, *30*, 409. Savin, A.; Nesper, R.; Wengert, S.; Fässler, T. F. *Angew. Chem., Int. Ed.* **1997**, *36*, 1809.
(22) Kaupp, M. *Chem. Ber.* **1996**, *129*, 527. Silvi, B.; Gatti, C. *J. Phys. Chem. A* **2000**, *104*, 947. Llusar, R.; Beltrán, A.; Andrés, J.; Fuster, F.; Silvi, B. *J. Phys. Chem. A* **2001**, *105*, 9460.
(23) The low ELF values for transition-metal bonding attractors may be rationalized by destructive interference effects due to the influence of occupied metal d orbitals in the ELF distribution (cf. Kohout, M.; Savin, A. *J. Comput. Chem.* **1997**, *18*, 1431).

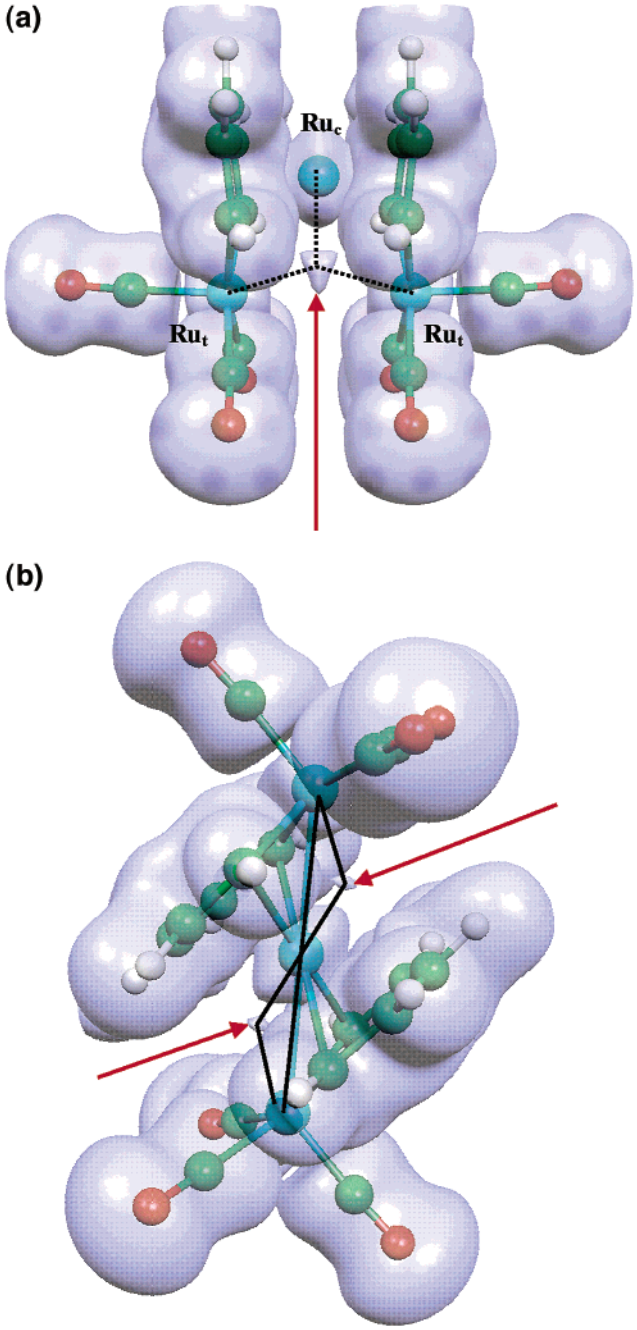

Figure 6. (a) ELF = 0.35 isosurface for [[η^6-pdRu(CO)$_3$]$_2$-Ru (obtained at the optimized structure). The three-center bonding attractor (with ELF$_{max}$ = 0.42) is marked by a red arrow. (b) Results for the anti conformer. The two disynaptic metal−metal bonding attractors (ELF = 0.38) are marked by a red arrow. The isosurfaces are displayed in a semitransparent way to allow the atoms and bonds to be seen.

those of benzene, suggesting a partial negative charge on the pd fragment in this particular case, as confirmed below by population analyses.

To act as an analogue to, for example, a cyclopentadienyl ligand in the formation of sandwich complexes, a metallabenzene has to exhibit frontier orbitals with similar nodal structures and orientations as found for other π-perimeter ligands.[24] The frontier orbitals of

(24) See, e.g.: Albright, T. A.; Burdett, J. K.; Whangbo, M. *Orbital Interactions in Chemistry*; Wiley: New York, 1985.

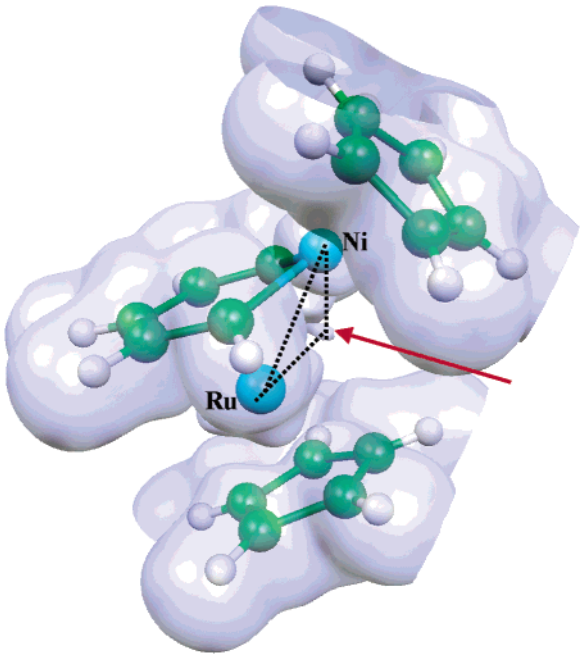

Figure 7. ELF = 0.35 isosurface for [{[η^6-pdNi(Cp)}-RuCp]$^+$ (obtained at the optimized structure). The metal−metal bonding attractor (with ELF$_{max}$ = 0.38) is marked by a red arrow. The isosurface is displayed in a semitransparent way to allow the atoms and bonds to be seen.

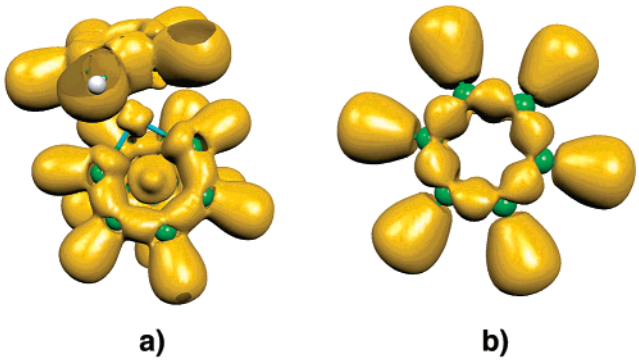

Figure 8. (a) Top view of ELF = 0.65 isosurface for [{η^6-pdNi(Cp)}RuCp]$^+$. (b) ELF = 0.65 isosurface for benzene.

metallabenzenes have been discussed in detail previously,[4,7] in particular regarding (a) their construction from the orbitals of the metal and pentadienyl fragments and (b) the factors that lead to C−C bond-length equalization within the ring. Figure 9 shows for [pdRu(CO)$_3$]$^-$ that the free metallabenzene anion exhibits a highest occupied molecular orbital (HOMO) with clear σ-donor character. The largest amplitude of this HOMO centers around the metal, the coordinating pentadiene carbon atoms C1 and C1′, and to a lesser extent also the equatorial carbonyl carbon atoms. This suggests that σ-donation should be most efficient when the coordinated metal center is held in close vicinity to the ring metal and its directly coordinated carbon atoms. The lowest unoccupied molecular orbital (LUMO) of the free metallabenzene exhibits appropriate symmetry for π-back-bonding (nodal planes between metal and C1, C1′, as well as between C2, C2′, and C3), thus underlining the analogy to benzene or cyclopentadienyl π-perimeter ligands. Again, the largest coefficients are clearly located on metal and C1 atoms. However, the LUMO also has significant amplitude on the C2 and C3

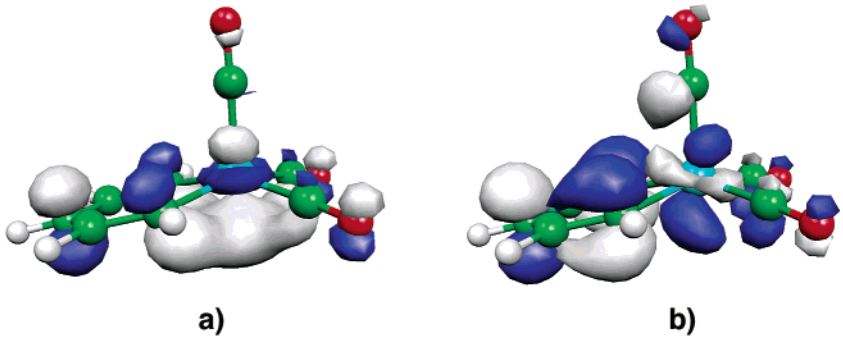

Figure 9. Frontier MOs of $[pdRu(CO)_3]^-$ (isosurface ±0.05 au): (a) HOMO; (b) LUMO.

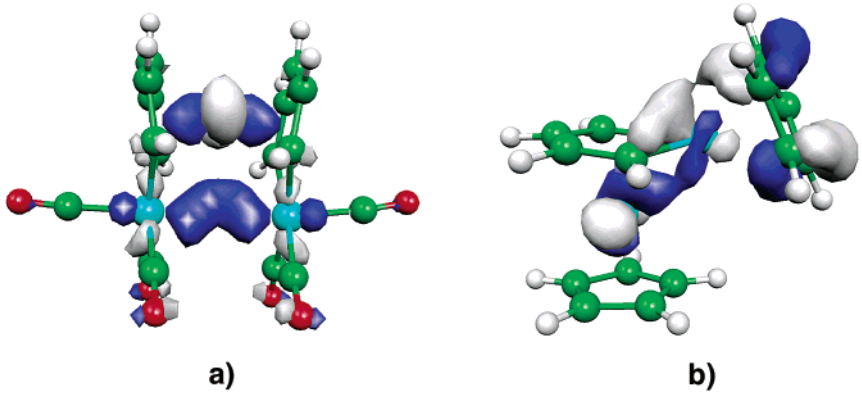

Figure 10. HOMO isosurfaces (±0.05 au): (a) $[[\eta^6\text{-}pdRu(CO)_3]_2Ru$ (**13a**); (b) $[\{\eta^6\text{-}pdNi(Cp)\}RuCp]^+$.

atoms. The π-back-bonding apparently would allow coordination to a metal center either in the observed way near C1 and metallabenzene metal or closer to the C2 and C3 atoms. In any case, inspection of the frontier MOs suggests clearly that the metal center and its close vicinity play a decisive role in the ligand properties of a metallabenzene. Frontier orbitals with similar nodal characteristics may be identified for the neutral [pdNi(Cp)] model fragment (not shown).

Figure 10 shows the HOMOs of both **13a** and $[\{\eta^6\text{-}pdNi(Cp)\}RuCp]^+$. In both systems, the orbital exhibits appreciable metal−metal bonding character. In the former case, the three-center bonding character identified in the ELF (see above and Figure 6) is reflected in the shape of the HOMO (all three metals are involved in a bonding fashion). In the latter case, the HOMO exhibits bonding interactions involving mainly the two metals and the C1 and C1′ atoms (some amplitudes on the Ni-coordinated Cp ligand are also notable). Lower occupied MOs show further bonding interactions between the metallabenzene ligand and the coordinated metal center. In all cases, the metal−metal antibonding contributions are mainly concentrated in the lowest unoccupied MOs (not shown), leaving a net bonding situation. That is, the analysis clearly shows (a) the analogy of the frontier MOs of a metallabenzene fragment to those of typical π-perimeter ligands and (b) a strong involvement of the ring metal center in the coordination to a further metal center. The large participation of the ring metal in the frontier orbitals of metallabenzenes make it likely that metal−metal bonding interactions of various types are a typical characteristic of the ligand properties of metallabenzenes. Exceptions may occur when the metals are bridged by some electrophile. Examples are known for hydride (proton) bridged metallabenzene complexes, where some of the metal−metal interactions are replaced by bridging M−H−M bonds.[4] In previous studies of ELF topology, sites of protonation have frequently been identified with the position of ELF attractors in the unprotonated species.[25] This suggests that the site of protonation in **13** or **13a** may be close to the three-center bonding attractor in the ELF. Indeed, DFT optimization of protonated **13a** (**13a-H**$^+$) gives a structure in which the proton is located on the bisector of the $Ru_t-Ru_c-Ru_t$ angle (Figure 11). While the Ru_t-Ru_c distances (Ru_t = terminal ruthenium atom, Ru_c = central ruthenium atom) remain almost unaltered upon protonation, the $Ru_t-Ru_c-Ru_t$ angle is increased by ca. 8° to ca. 85°, leading to an expanded Ru_t-Ru_t distance of ca. 3.85 Å. The M−H distances are somewhat longer than suggested by the position of the ELF-attractor computed for **13a**. A preliminary DFT calculation of the ^{1}H chemical shift of the metal-bonded hydride, using the spin−orbit-corrected approach detailed in ref 26, gave −17.1 ppm (with a sizable spin−orbit contribution of −4.4 ppm), in reasonable agreement with the measured −16.1 ppm (see above).

Table 4 summarizes the partial atomic and fragment charges obtained from natural population analyses (NPA) for two d^8 metallabenzene fragments and their associated complexes. First of all, charge donation from the formal d^8 fragments to the central metal is signifi-

(25) See, e.g.: Fuster, F.; Silvi, B. *Chem. Phys.* **2000**, *252*, 279. Similar to the description in that work, in the present case the formerly unprotonated ELF attractor is replaced by an attractor connected to the hydrogen atom (i.e., the number of attractors is conserved during the protonation; data not shown). For the protonation of a trisynaptic attractor see, e.g.: Binder, H.; Kellner, R.; Vaas, K.; Hein, M.; Baumann, F.; Wanner, M.; Kaim, W.; Wedig, U.; Hönle, W.; von Schnering, H. G.; Groeger, O.; Engelhardt, G. *Z. Anorg. Allg. Chem.* **1999**, *625*, 1638.

(26) Vaara, J.; Malkina, O. L.; Stoll, H.; Malkin, V. G.; Kaupp, M. *J. Chem. Phys.* **2001**, *114*, 61.

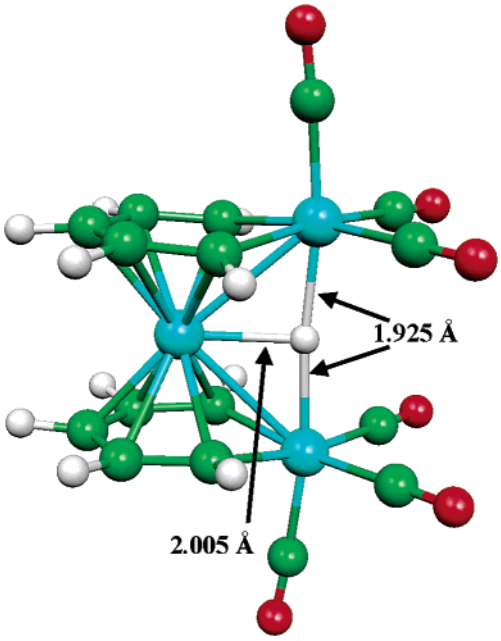

Figure 11. Optimized structure of protonated **13a** (**13a-H**$^+$). $d(Rh_t-Rh_t) = 3.851$ Å, $d(Rh_t-Rh_c) = 2.854$ Å.

Table 4. Natural Atomic and Fragment Charges[a]

	[pdNi(Cp)]	[{pdNi(Cp)}-RuCp]$^+$	[pdRu-(CO)$_3$]$^-$	[pdRu(CO)$_3$]$_2$-Ru
Ni(ring)	0.739	0.784		
Ru$_c$(central)	−	0.101		0.015
Ru$_t$ (ring)			−0.197	−0.282
C1(pd)	−0.317	−0.373	−0.453	−0.397
C2(pd)	−0.347	−0.233	−0.325	−0.235
C3(pd)	−0.110	−0.190	−0.219	−0.215
H(C1)	0.228	0.255	0.192	0.246
H(C2)	0.199	0.279	0.196	0.256
H(C3)	0.226	0.283	0.201	0.263
Cp(Ni)	−0.382	−0.125		
Cp(Ru)		0.291		
CO$_{eq}$			−0.011	+0.143
CO$_{ax}$			+0.016	+0.203
total (metallabenzene)	0.000	+0.608	−1.000	−0.005

[a] Obtained from natural population analyses (NPA) of the B3PW91 Kohn−Sham orbitals.

cant in both cases. Not surprisingly, it is more pronounced for the negatively charged fragment [Ru(pd)(CO)$_3$]$^-$. This suggests that in all systems studied here, the σ-donation from the HOMO of the metallabenzene (cf. Figure 9) to appropriate empty orbitals of the central metal dominates the interactions, whereas π-back-bonding is probably less pronounced. This provides a particularly convincing explanation for the observed preference to form metal−metal bonds, as the HOMO does generally exhibit particularly large ring−metal character. Closer inspection of the fragment charges indicates that not only is the metallabenzene ring itself involved in the charge donation but also the ancillary ligands (Cp in the nickelabenzene, carbonyl ligands in the ruthenabenzene). Of the atoms in the metallabenzene fragment, charge withdrawal from the C2 atoms and from the hydrogen atoms is most apparent, whereas no clear-cut trend may be discerned for the metal and C1 atoms, and the C3 atoms appear to even receive some charge. These observations reflect the partial compensation of σ-donation from and π-back-donation to the metallabenzene.

Experimental Section

All reactions were performed under nitrogen using Schlenk techniques. Solvents were dried and deoxygenated by standard procedures. Chromatography was carried out with Merck silica gel 60. NMR spectra were recorded on a Varian Mercury VXR (300 MHz, ^{1}H; 75 MHz, ^{13}C) and a Varian Unity 500 (500 MHz, ^{1}H; 125 MHz, ^{13}C) at ambient temperature. Chemical shifts (δ) are given in ppm relative to $SiMe_4$. Melting points were measured on a Heidolph/Kelheim Typ 101.30 apparatus. IR spectra were recorded on a Perkin-Elmer FT-IR Model 1720 X spectrometer. Mass spectra were obtained with a Finnigan MAT 95 spectrometer. Elemental analyses were obtained on a Carlo Erba Strumentazione Element Analyzer, Model 1106. Dimethylpentadiene and trimethylpentadiene were prepared by standard methods and **3** and **4**,[1] **5**,[18] **6**,[19] and **7** and **8**[20] according to published procedures.

Details of Quantum Chemical Calculations. We have fully optimized the structures of the following complexes: (a) the as yet experimentally unknown "free" d^8 metallabenzene fragments [Ru(pd)(CO)$_3$]$^-$ and [pdNi(Cp)] (pd = pentadienylylidene, C_5H_5), the metallabenzene-sandwich complexes [η^6-pdRu(CO)$_3$]$_2$Ru (**13a**), [[η^6-dpdRu(CO)$_3$]$_2$Ru (**13**; dpd = 2,4-dimethylpentadienylylidene, C_7H_9), and [{η^6-pdNi(Cp)}RuCp}$^+$. **13a** is a simplified model of **13**, and the Ni complex is a simplified model of the experimentally characterized complex [{η^6-dpdNi(Cp)}RuCp*]$^+$.[2] No symmetry restrictions were applied in these optimizations and in the optimization of (**13a-H**$^+$). Optimization of the less stable anti conformer of **13a** employed C_s symmetry.

All structure optimizations and electronic-structure analyses have been carried out using density functional theory, employing the B3PW91 hybrid functional.[27] The Gaussian98 program[28] was used throughout this work. Quasi-relativistic small-core pseudopotentials (effective-core potentials, ECPs) and [8s7p6d]/(6s5p3d) valence basis sets were used for the transition metals,[29] as well as ECPs and DZP valence basis sets for C and O[30] and a DZV basis for hydrogen.[31]

The electronic structure of the complexes has been studied using three different means: (a) analyses of the electron localization function (ELF);[21] (b) natural population analyses (NPA[32]) (using the built-in NBO module of the Gaussian98 program);[28] (c) visualization of the canonical Kohn−Sham frontier orbitals. The ELF data have been created and

(27) (a) Becke, A. D. *J. Chem. Phys.* **1993**, *98*, 5648. Perdew, J. P.; Wang, Y. *Phys. Rev. B* **1992**, *45*, 13244. (b) Perdew, J. P. In *Electronic Structure of Solids*; Ziesche, P., Eischrig, H., Eds.; Akademie Verlag: Berlin, 1991. Perdew, J. P.; Chevary, J. A.; Vosko, S. H.; Jackson, K. A.; Pederson, M. R.; Singh, D. J.; Fiolhais, C. *Phys. Rev. B* **1992**, *46*, 6671.

(28) Frisch, M. J.; Trucks, G. W.; Schlegel, H. B.; Scuseria, G. E.; Robb, M. A.; Cheeseman, J. R.; Zakrzewski, V. G.; Montgomery, J. A., Jr.; Stratmann, R. E.; Burant, J. C.; Dapprich, S.; Millam, J. M.; Daniels, A. D.; Kudin, K. N.; Strain, M. C.; Farkas, O.; Tomasi, J.; Barone, V.; Cossi, M.; Cammi, R.; Mennucci, B.; Pomelli, C.; Adamo, C.; Clifford, S.; Ochterski, J.; Petersson, G. A.; Ayala, P. Y.; Cui, Q.; Morokuma, K.; Malick, D. K.; Rabuck, A. D.; Raghavachari, K.; Foresman, J. B.; Cioslowski, J.; Ortiz, J. V.; Stefanov, B. B.; Liu, G.; Liashenko, A.; Piskorz, P.; Komaromi, I.; Gomperts, R.; Martin, R. L.; Fox, D. J.; Keith, T.; Al-Laham, M. A.; Peng, C. Y.; Nanayakkara, A.; Gonzalez, C.; Challacombe, M.; Gill, P. M. W.; Johnson, B. G.; Chen, W.; Wong, M. W.; Andres, J. L.; Head-Gordon, M.; Replogle, E. S.; Pople, J. A. *Gaussian 98*, revision A.7; Gaussian, Inc.: Pittsburgh, PA, 1998.

(29) Dolg, M.; Wedig, U.; Stoll, H.; Preuss, H. *J. Chem. Phys.* **1987**, *86*, 866. Andrae, D.; Häussermann, U.; Dolg, M.; Stoll, H.; Preuss, H. *Theor. Chim. Acta* **1990**, *77*, 123.

(30) Bergner, A.; Dolg, M.; Küchle, W.; Stoll, H.; Preuss, H. *Mol. Phys.* **1993**, *80*, 1431. (b) d-functions were taken from: *Gaussian Basis Set for Molecular Calculations;* Huzinaga, S., Ed.; Elsevier: New York, 1984.

(31) Godbout, N.; Salahub, D. R.; Andzelm, J.; Wimmer, E. *Can. J. Chem.* **1992**, *70*, 560.

(32) Reed, A. E.; Weinhold, F. *J. Chem. Phys.* **1985**, *83*, 1736. Reed, A. E.; Curtiss, L. A.; Weinhold, F. *Chem. Rev.* **1988**, *88*, 899.

analyzed using the TopMoD suite of programs.[33] Both ELF and frontier orbitals are graphically displayed using the Molekel program.[34]

X-ray Structure Determination of 9, 11 and 14. Geometry and intensity data were collected with Mo Kα radiation on an Enraf-Nonius CAD4 diffractometer equipped with a graphite monochromator. A summary of crystal data, data collection parameters, and convergence results is compiled in Table 1. Empirical absorption corrections based on azimuthal scans[35] were applied before averaging symmetry-equivalent data. The structures were solved by direct methods[36] and subsequent Fourier difference syntheses. The models were refined on intensities.[37] In the full-matrix least-squares refinement, all non-hydrogen atoms were assigned anisotropic displacement parameters. In the case of **11**, hydrogen atoms in the open pentadienyl ligand were refined with isotropic displacement parameters. All remaining H atoms were treated as riding on the corresponding carbon atoms. Further details on the structure determination are available from the Cambridge Crystallographic Data Center: CCDC-196643 (for **9**), CCDC-196644 (for **11**), and CCDC-196645 (for **14**).

(η^5-2,4-Dimethylpentadienyl)(η^5-pentamethylcyclopentadienyl)iron (1). $FeBr_2$·DME (11.1 g, 36 mmol) was suspended in THF (100 mL). A mixture of freshly prepared sodium pentamethylcyclopentadienide (36 mmol) and potassium 2,4-dimethylpentadienide (36 mmol) in THF was added dropwise at −78 °C. The cold bath was removed and the solution warmed overnight to room temperature. The solvent was evaporated, the residue taken up in hexane, and the solution filtered over Celite. The solvent was evaporated again, and a minimum amount of hexane was added. At −30 °C a mixture of compounds was crystallized and the supernatant liquid was decanted. The 5-fold minimum amount of hexane was used to dissolve the residue. With very slow cooling to −20 °C, the half-open ferrocene was crystallized and isolated. Yield: 1.9 g (18%). ^{1}H NMR (300 MHz, C_6D_6): 4.64 (s, 1H, H-3), 2.00 (s, 1H, H-1), 1.85 (s, 6H, H-4), 1.59 (s, 15H, C_5Me_5), −0.52 (s, 1H, H-1′). ^{13}C NMR (75 MHz, C_6D_6): 93.5 (C-2), 89.8 (C-3), 84.4 (C_5), 46.4 (C-1), 25.1 (C-4), 10.5 (Me_5). Anal. Calcd (found) for $C_{17}H_{26}Fe$: C, 71.33 (71.33); H, 9.16 (9.47).

(η^5-2,4-Trimethylpentadienyl)(η^5-pentamethylcyclopentadienyl)iron (2). The procedure was identical with that described before, starting from $FeBr_2$·DME (14.8 g, 43 mmol), sodium pentamethylcyclopentadienide (43 mmol), and potassium 2,3,4-trimethylpentadienide (43 mmol). After the mixture of compounds was crystallized and the supernatant liquid was discarded, the 5-fold minimum amount of hexane was used to dissolve the mixture. Slow cooling to −20 °C gave a precipitate of decamethylferrocene. The supernatant liquid was withdrawn with a syringe, reduced in volume, and cooled to −30 °C. Crystals of **2** separated. When the volume of the solvent was reduced further, a second crop of crystals was obtained. Yield: 1.5 g (12%). ^{1}H NMR (500 MHz, C_6D_6): 2.08 (s, 1H, H-1), 1.83 (s, 6H, H-4), 1.82 (s, 3H, H-5), 1.56 (s, 15H, C_5Me_5), −0.62 (s, 1H, H-1′). ^{13}C NMR (125 MHz, C_6D_6): 96.2 (C-3), 90.4 (C-2), 84.1 (C_5), 49.4 (C-1), 24.4 (C-4), 10.2 (Me_5). Anal. Calcd (found) for $C_{18}H_{28}Fe$: C, 72.00 (72.44); H, 9.40 (9.60).

Tetracarbonyl(η^5-2,4-dimethylpentadienyl)(η^5pentamethylcyclopentadienyl)iron−ruthenium (9). To compound **3** (0.33 g, 1 mmol), dissolved in 30 mL of benzene, was added nonacarbonyldiiron (0.37 g, 1 mmol). The reaction mixture was stirred at 60 °C for 24 h. The solvent and excess iron carbonyl (*Caution!* Iron carbonyl is very poisonous. The use of two efficient cold traps is recommended.) were evaporated under reduced pressure. The residue was extracted with warm hexane and the extract cooled to −30 °C. Red crystals of **9** separated. If necessary, further purification by chromatography over Al_2O_3 (activity grade II−III) with toluene as eluent was possible. Yield: 0.4 g, 80%. IR (hexane): ν_{max} 1969, 1946, 1767 (CO) cm^{-1}. ^{1}H NMR (500 MHz, C_6D_6): 4.24 (s, 1H, H-3, 3.33 (s, 2H, H-1′), 1.93 (s, 6H, H-4, 1.62 (s, 15 H, C_5Me_5), 0.97 (s, 2H, H-1). ^{13}C NMR (125 MHz, C_6D_6): 116.7 (C-2), 101.5 (C_5), 97.3 (C-3), 63.9 (C-1), 24.4 (C-4) 9.0 (Me_5). MS (EI): 500 (20%, M^+), 444 (16%, $M^+ - 2CO$), 416 (2%, $M^+ - 3CO$), 384 (100%, $C_{17}H_{22}FeRu^+$), 293 (17%, $C_5Me_5Ru(CO)_2^+$), 265 /15%, $C_5Me_5RuCO^+$), 237, (12%, $C_5Me_5Ru^+$), 151 (5%, $C_7H_{11}Fe^+$). Anal. Calcd (found) for $C_{21}H_{26}FeO_4Ru$: C, 50.51 (50.61), H, 5.25 (5.34).

Tetracarbonyl(η^5-2,4-trimethylpentadienyl)(η^5-pentamethylcyclopentadienyl)iron−ruthenium (10). 10 was prepared similarly to **9** from **4** (0.35 g, 1 mmol) and nonacarbonyldiiron (0.41 g, 1.1 mmol). The raw product was extracted with toluene and purified by chromatography over Al_2O_3 (II−III). The orange fraction was collected and evaporated. The dry residue was dissolved in warm hexane and cooled to −30 °C. Red-orange crystals of **10** separated (0.38 g, 39%). IR (hexane): ν_{max} 1966, 1927, 1753 (CO) cm^{-1}. ^{1}H NMR (500 MHz, C_6D_6): 3.24 (s, 2H, H-1), 1.92 (s, 6H, H-4), 1.71 (s, 3H, H-5), 1.65 (s, 15 H, C_5Me_5), 0.78 (s, 2H, H-1′). ^{13}C NMR (125 MHz, C_6D_6): 113.3 (C-2), 109.6 (C-3), 101.6 (C_5), 65.6 (C-1), 24.7 (C-4), 17.0 (C-5), 9.0 (Me_5). MS (SIMS): 514 (16%, M^+), 486 (14%, $M^+ - CO$), 458 (54%, $M^+ - 2CO$), 321 (33%, $C_5Me_5Ru(CO)_3^+$), 293 (74%, $C_5Me_5(CO)_2^+$), 265 (12%, $C_5Me_5CO^+$). Anal. Calcd (found) for $C_{22}H_{28}FeO_4Ru$: C, 51.47 (51.41), H, 5.50 (5.56).

***cis*-(μ-(1,4,5η):(1−3η)-2,4-dimethylpentadienediyl)bis(tricarbonyliron) (11).** Bis(2,4-dimethylpentadienyl)iron (**5**; 0.71 g, 2.9 mmol) was dissolved in benzene (90 mL) and treated with nonacarbonyldiiron (2.1 g, 5.8 mmol). The reaction mixture was stirred at 60 °C for 1 day. Solvent and iron pentacarbonyl were removed under reduced pressure (*Caution!* efficient cold trap). The residue was taken up in hexane and the solution filtered over Celite. The concentrated hexane solution was then purified over silica gel. The orange-red fraction was collected and evaporated. The dry residue was sublimed at 50 °C under high vacuum. A total of 0.55 g (1.5 mmol, 51%) was obtained. IR (hexane): ν_{max} 2064, 2022, 1991, 1973 (CO) cm^{-1}. ^{1}H NMR (500 MHz, C_6D_6): 6.68 (d, ^4J = 2.7 Hz, 1H, H-5), 3.77 (d, ^4J = 2.4 Hz, 1H, H-3), 1.66 (s, 3H, Me), 1.07 (s, 3H, Me), 0.88 (s, 1H, H-1), 0.69 (s, 1H, H-1′). ^{13}C NMR (125 MHz, C_6D_6): 212.5 (CO), 211.5 (CO), 147.3 (C-5), 110.7 (C-4), 97.3 (C-2) 68.9 (C-3), 45.1 (C-1), 25.7 (Me), 22.4 (Me). MS (EI): *m/z* 374 (12%, M^+), 346 (34%, $M^+ - CO$), 318 (18%, $M^+ - 2CO$), 290 (24%, $M^+ - 3CO$), 262 (25%, $M^+ - 4CO$), 234 (63%, $M^+ - 5$ CO), 206 (100%, $M^+ - 6CO$). Anal. Calcd (found) for $C_{13}H_{10}Fe_2O_6$: C, 41.76 (41.79), H, 2.70 (2.71).

***cis*-(μ-(1,4,5η):(1−3η)-2,3,4-trimethylpentadienediyl)bis(tricarbonyliron) (12).** Bis(2,3,4-trimethylpentadienyl)iron (**6**; 0.135 g, 0.5 mmol) was dissolved in benzene (30 mL) and treated with nonacarbonyldiiron (0.364 g, 1 mmol) as described above. After workup and chromatography a concentrated hexane solution was cooled to −80 °C. Orange-red crystals separated (0.1 g, 0.26 mmol, 52%). IR (hexane): ν_{max} 2063, 2021, 1981, 1962 (CO) cm^{-1}. ^{1}H NMR (500 MHz, C_6D_6): 6.57 (s, 1H, H-5), 1.73 (s, 3H, Me), 1.47 (s, 3H, Me), 1.04 (s, 3H, Me), 0.97 (s, 1H, H-1) 0.50 (s, 1H, H-1′). ^{13}C NMR (125 MHz, C_6D_6): 212.5 (CO), 211.6 (CO), 145.3 (C-5), 109.1 (C-4), 98.9 (C-2) 80.3 (C-3), 44.7 (C-1), 25.2 (Me), 21.2 (Me), 21.1 (Me). MS (EI): *m/z* 388 (10%, M^+), 360 (14%, $M^+ - CO$), 332 (15%, $M^+ - 2CO$), 304 (26%, $M^+ - 3CO$), 276 (28%, $M^+ - 4CO$), 248 (44%, $M^+ - 5$ CO), 220 (100%, $M^+ - 6CO$). Anal. Calcd (found) for $C_{14}H_{12}Fe_2O_6$: C, 43.35 (43.23); H, 3.12 (3.19).

(33) Noury, S.; Krokidis, X.; Fuster, F.; Silvi, B., TopMoD package; Université Pierre et Marie Curie, 1997.
(34) Flükiger, P.; Lüthi, H. P.; Portmann, S.; Weber, J. Molekel 4.0; Swiss Center for Scientific Computing, Manno, Switzerland, 2000. See, e.g.: Portmann, S.; Lüthi, H. P. *Chimia* **2000**, *54*, 766.
(35) North, A. C. T.; Phillips, D. C.; Mathews, F. S. *Acta Crystallogr., Sect. A* **1968**, *24*, 351.
(36) Sheldrick, G. M. SHELXS86, Program for Crystal Structure Solution; University of Göttingen, Göttingen, Germany, 1986.
(37) Sheldrick, G. M. SHELXL97, Program for Crystal Structure Refinement; University of Göttingen, Göttingen, Germany, 1997.

Bis(η^6-3,5-dimethyl-1-tricarbonylruthenabenzene)ruthenium (13). A solution of 0.29 g (1 mmol) of bis(2,4-dimethylpentadienyl)ruthenium (**7**), dissolved in 35 mL of octane, was treated with 1.28 g (2 mmol) of dodecacarbonyltriruthenium and heated under reflux overnight. After evaporation of the solvent, the dry black residue was extracted with hexane and purified via chromatography over SiO_2. A yellow fraction was collected. The solvent was evaporated and the dry residue recrystallized from benzene or toluene, yielding yellow crystals after a few hours; yield 0.12 g, 18%. IR (hexane): ν_{max} 2074, 2049, 2010, 1995, 1980 (CO) cm^{-1}. ^1H NMR (500 MHz, CD_2Cl_2): 6.23 (t, ^4J = 1.5 Hz, 2H, H-3), 5.62 (d, ^4J = 1.5 Hz, 4H, H-1), 1.73 (s, 12H, H-4). ^{13}C NMR (125 MHz, CD_2Cl_2): 198.9 (CO), 193.9 (CO), 128.3 (C-1), 111.4 (C-2), 94.4 (C-3), 25.5 (Me). MS (EI): 657 (6%, M^+), 629 (7%, $M^+ - CO$), 601 (13%, $M^+ - 2CO$), 573 (14%, $M^+ - 3CO$), 545 (23%, $M^+ - 4CO$), 517 (10%, $M^+ - 5CO$), 489 (13%, $M^+ - 6CO$), 388 (9%, $M - Ru(CO)_6$), 288 (100%, $(C_7H_9)_2Ru^+$), 273 (43%, $(C_7H_9)_2Ru^+ - Me$), 195 (11%, $(C_7H_9)Ru^+$). Anal. Calcd (found) for $C_{20}H_{18}O_6Ru_3$: C, 36.52 (36.48), H, 2.76 (2.80).

Bis(η^6-3,4,5-trimethyl-1-tricarbonylruthenabenzene)ruthenium (14). A solution of bis(2,3,4-trimethylcyclopentadienyl)ruthenium (**8**; 0.6 g, 1.9 mmol), dissolved in 30 mL of nonane, was treated with 2.4 g (3.8 mmol) of $Ru_3(CO)_{12}$. The solution was refluxed overnight. After evaporation of the solvent, the black residue was extracted with methylene chloride and filtered over silica gel. After evaporation of methylene chloride, the solid was recrystallized from benzene. The resulting crystals were still a mixture of the product and $Ru_3(CO)_{12}$. This mixture was washed with methylene chloride, yielding a yellow solid. This was again recrystallized from benzene and gave 0.04 g (5%) yield of **13**. IR (hexane): ν_{max} 2070, 2045, 2007, 1990, 1975 (CO) cm^{-1}. ^1H NMR (300 MHz, C_6D_6): 5.39 (s, 2H, H-1), 1.24 (s, 3H, H-5), 0.93 (s, 6H, H-4). ^{13}C NMR (75 MHz, C_6D_6): 199.0 (CO), 194.4 (CO), 130.9 (C-1), 110.2 (C-2), 104,2 (C-3), 24.6 (Me), 17.5 (Me). Anal. Calcd (found) for $C_{22}H_{22}O_6Ru_3$: C, 38.54 (38.38); H, 3.23 (3.30).

(η^5-2,4-Dimethylpentadienyl)(η^6-3,5-dimethyl-1-tricarbonylruthenabenzene)ruthenium (15). An octane solution of 0.59 g (2.0 mmol) of **7** was treated with 1.41 g (2.2 mmol) of $Ru_3(CO)_{12}$ and refluxed overnight. Workup as with **13** yielded 0.08 g (1%) of yellow needles. IR (hexane): ν_{max} 2076, 2043, 2005, 2000, 1983 (CO) cm^{-1}. ^1H NMR (500 MHz, CD_2Cl_2): 6.57 (s, 2H, H-2,6), 4.35 (s, 2H, H-4, H-3′), 2.20 (s, 6H, Me), 2.10 (d, ^2J = 1.53 Hz, 2H, H-1′$_{exo}$), 1.85 (s, 6H, Me′), 1.67 (d, ^2J = 1.53 Hz, 2H, H1′$_{endo}$). ^{13}C NMR (125 MHz, CD_2Cl_2): 198 (CO), 197 (CO), 128.9 (C-2,6), 110.6 (C-3,5), 104.5 (C-2′), 59.8 (C-4,3′), 44.0 (C-1′), 27.2 (Me), 24.3 (Me′). Anal. Calcd (found) for $C_{17}H_{20}O_3Ru_2$: C, 43.03 (43.20), H, 4.24 (4.32).

Protonation of 13. A 215 mg portion of **13** was dissolved in ether and cooled to −30 °C. After addition of 0.135 mL (0.98 mmol) of $HBF_4 \cdot OEt_2$ the solution was stirred and then warmed slowly. The white solid that initially formed dissolved again, leaving a yellow solution. Then a yellow precipitate was formed, which again dissolved around 0 °C. The yellow solution was evaporated in vacuo, giving a yellow-orange precipitate, which was washed with ether. In attempts to grow single crystals from CD_3NO_2, the compound slowly releases HBF_4 and **13** is re-formed. ^1H NMR (80 MHz, CD_3CN): 6.34 (s, 2H, H-3), 6.09 (s, 4h, H-1), 1.28 (s, 12 H, Me), −16.89 (s, 1H, Ru−H).

Supporting Information Available: Tables giving X-ray crystallographic data for **9**, **11**, and **14**. This material is available free of charge via the Internet at http://pubs.acs.org.

OM020789H